LA-UR-12-24002
Approved for public release; distribution is unlimited.

Title: Bulk and surface controlled diffusion of fission gas atoms

Author(s): Andersson, Anders D.

Intended for: Report

# Bulk and surface controlled diffusion of fission gas atoms

David Andersson
Los Alamos National Laboratory, Los Alamos, NM 87545, USA

## Introduction

Fission gas retention and release impact nuclear fuel performance by, e.g., causing fuel swelling leading to mechanical interaction with the clad, increasing the plenum pressure and reducing the gap thermal conductivity. All of these processes are important to understand in order to optimize operating conditions of nuclear reactors and to simulate accident scenarios. Most fission gases have low solubility in the fuel matrix, which is especially pronounced for large fission gas atoms such as Xe and Kr, and as a result there is a significant driving force for segregation of gas atoms to extended defects such as grain boundaries or dislocations and subsequently for nucleation of gas bubbles at these sinks.

Several empirical or semi-empirical models have been developed for fission gas release in nuclear fuels, e.g. [1-6]. One of the most commonly used models in fuel performance codes was published by Massih and Forsberg [3,4,6]. This model is similar to the early Booth model [1] in that it applies an equivalent sphere to separate bulk $UO_2$ from grain boundaries represented by the sphere circumference. Compared to the Booth model, it also captures trapping at grain boundaries, fission gas resolution and it describes release from the boundary by applying time-dependent boundary conditions to the circumference. In this work we focus on the step where fission gas atoms diffuse from the grain interior to the grain boundaries. The original Massih-Forsberg model describes this process by applying an effective diffusivity divided into three temperature regimes [3,4,7].

$$D_1 = 1.09 \cdot 10^{-17} \exp\left(-0.57/k_B T\right) m^2/s \quad T > 1650\,K$$
$$D_2 = 2.14 \cdot 10^{-13} \exp\left(-1.97/k_B T\right) m^2/s \quad 1381 < T < 1650\,K \quad \text{(Equation 1)}$$
$$D_3 = 1.51 \cdot 10^{-17} \exp\left(-0.82/k_B T\right) m^2/s \quad T < 1381K$$

In a later publication [5] they replaced the earlier model with a revised version derived by Turnbull [8-10].

$$D_1 = 7.6 \cdot 10^{-10} \exp\left(-3.04/k_B T\right) m^2/s \quad T > 1650\,K$$
$$D_2 = 4 \times 1.41 \cdot 10^{-25} \times \sqrt{\dot{F}} \exp\left(-1.20/k_B T\right) m^2/s \quad 1381 < T < 1650\,K \quad \text{(Equation 2)}$$
$$D_3 = 4 \times 2 \cdot 10^{-40} \dot{F}\, m^2/s \quad T < 1381K$$

Here $\dot{F}$ is the fission rate. Obviously, there are significant differences between these models (especially the pre-exponentials and the activation energies). In this report, we will not necessarily focus on the differences between these models, but it is

worth noting that the differences exist (and the implication is that there is an opportunity to improve the manner in which fission gas behavior is modeled in fuel performance codes). Rather, in his report, we revisit the original data which these models were derived to fit, and attempt to provide important interpretations of the different diffusion mechanisms dominant in three different regimes by comparing the data to DFT. In the Turnbull model [8-10], the three temperature regimes correspond to A) athermal diffusion (below 1381 K) where transport is caused directly by irradiation damage ($D_3$), B) irradiation enhanced diffusion ($D_2$), presumably due to increased concentration of vacancies (for 1381<T<1650 K), and C) intrinsic diffusion controlled by thermally generated defects ($D_1$) (for T>1650 K). Fig. 1 illustrates the diffusivity as function temperature according to Turnbull's model. For the intrinsic regime (denoted by the red line in Fig, 1), Turnbull used the diffusivity determined by Davies and Long [11]. However, there are uncertainties associated with this experimental number, as evidenced by the fact that Matzke suggested a significantly higher value (3.9 eV compared to 3.09 eV) for this regime [12]. The DFT calculations should enable us to better interpret the physical mechanisms that are responsible for the diffusivities determined by Turnbull.

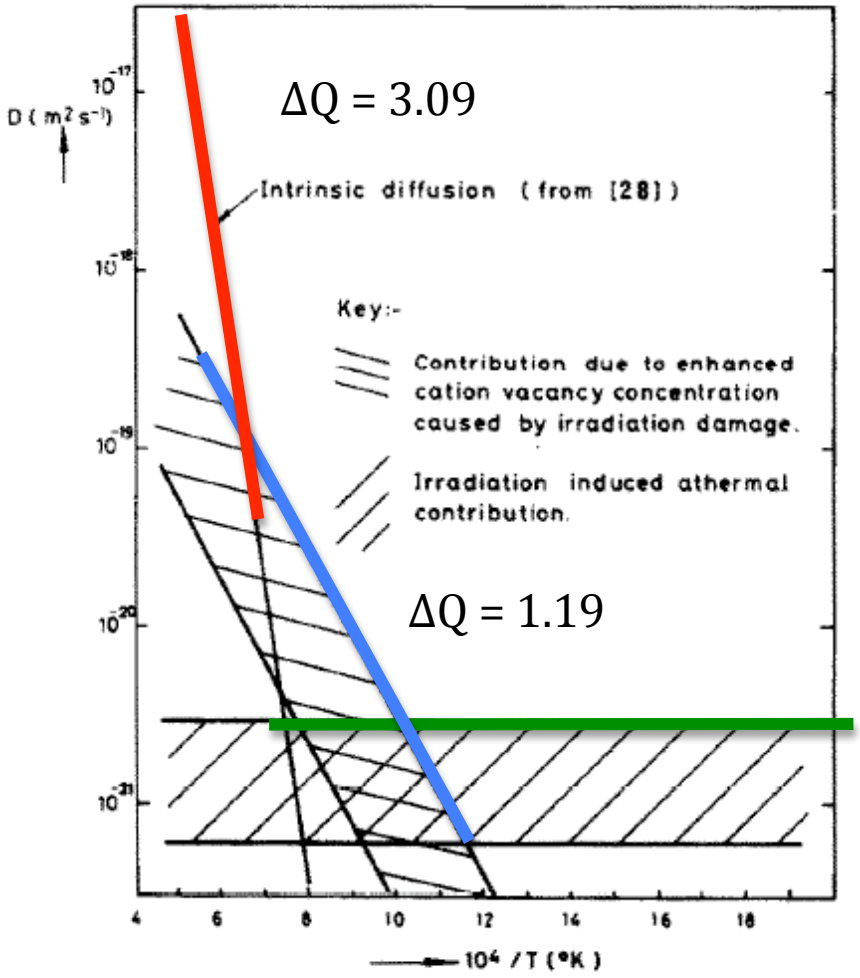


**Figure 1: The in-pile fission gas diffusivity as function of temperature according to Turnbull [8-10]. The figure is reproduced from Ref. [8].**

In this report we present results from density functional theory calculations (DFT) that are relevant for the high ($D_3$) and intermediate ($D_2$) temperature diffusivities of fission gases. The results are validated by making a quantitative comparison to Turnbull's [8-10] and Matzke's data [12]. For the intrinsic or high temperature regime we report activation energies for both Xe and Kr diffusion in $UO_{2\pm x}$, which compare favorably to available experiments. This is an extension of previous work [13]. In particular, it applies improved chemistry models for the $UO_{2\pm x}$ non-stoichiometry and its impact on the fission gas activation energies. The derivation of these models follows the approach that used in our recent study of uranium vacancy diffusion in $UO_2$ [14]. Also, based on the calculated DFT data we analyze vacancy enhanced diffusion mechanisms in the intermediate temperature regime. In addition to vacancy enhanced diffusion we investigate species transport on the (111) $UO_2$ surface. This is motivated by the formation of small voids partially filled with fission gas atoms (bubbles) in $UO_2$ under irradiation, for which surface diffusion could be the rate-limiting transport step. Diffusion of such bubbles constitutes an alternative mechanism for mass transport in these materials.

## Activation energies for Xe and Kr diffusion in $UO_{2\pm x}$

In our previous study of Xe diffusion in $UO_{2\pm x}$ [13] we calculated the relevant defect formation energies, binding energies and migration barriers needed for estimating the activation energy for diffusion. These values are summarized in Table 1. The activation energies were obtained by using the point defect model that was originally derived by Matzke [12]. This model assumes that the non-stoichoimetry ($x$ in $UO_{2\pm x}$) is fixed and that it does not change with temperature. In order to fulfill these conditions in experiments, the oxygen partial pressure must be controlled and varied with the temperature. The change in non-stoichiometry is important since it directly controls the concentration of uranium vacancies, which is key to fission gas transport in these materials. However, the experiments due to Miekeley and Felix [15] that were used to validate the simulation results did not employ such an elaborate setup, but rather the oxygen partial pressure was controlled by the chemistry of the carrier gas and for this reason the nonstoichiometry was a function of temperature even within the $UO_{2-x}$, $UO_2$ and $UO_{2+x}$ regimes separated out in their analysis. In order to compare directly with these experiments a point defect model is required that correctly captures the chemistry. Such a model was derived for uranium diffusion in close to stoichiometric $UO_2$ in our recent study [13]. Here we apply a similar model for Xe and Kr diffusion and derive corresponding models for $UO_{2-x}$ and $UO_{2+x}$.

In [13] the following expression was derived for the activation energy for diffusion of U vacancies:

$$E_a^{V_U} = 2E_{O_I} + E_S - 2E_{eh} - 2E_{FP_O} + E_{p_{O_2}} + E_m^{V_U} \quad \textbf{(Equation 3)}$$

Here, $E_{O_I}$ is the $UO_2$ oxidation energy (interstitial formation energy), $E_S$ is the Schottky energy, $E_{eh}$ is the electron-hole pair formation energy, $E_{FP_O}$ is the oxygen

Frenkel pair energy, $E_{p_{O2}}$ is the activation energy controlling the oxygen partial pressure and $E_m^{V_U}$ is the uranium vacancy migration energy. The corresponding expression for Xe (or Kr) diffusion is obtained by adding the binding energy of U vacancies to the Xe trap site ($E_B$) and replacing the U migration barrier by the barrier for intra-cluster migration of the U vacancy that is bound to the Xe trap site ($E_m^{V_U,C}$) [13].

$$E_a^{Xe} = 2E_{O_I} + E_S - 2E_{eh} - 2E_{FP_O} + E_{p_{O2}} + E_m^{V_U,C} - E_B \quad \textbf{(Equation 4)}$$

Based on previous results we assume that Xe prefers the $V_{UO}$ (one U and one O vacancy bound together) trap site near stoichiometric $UO_2$. The binding energy and migration barriers in the above equation should be adjusted accordingly.

It is reasonable to assume that reduction of $UO_{2-x}$ occurs via $2U_U^X + O_O^X \Leftrightarrow 2e' + V_O^{\bullet\bullet} + \frac{1}{2}O_2(g)$ ($E_1$) and from this we derive the following expression for the activation energy in the $UO_{2-x}$ range:

$$E_a^{Xe} = E_S + \frac{E_{p_{O2}}}{3} - \frac{2E_1}{3} + E_m^{V_U,C} - E_B \quad \textbf{(Equation 5)}$$

For $UO_{2-x}$ Xe atoms occupy the $V_{UO2}$ (one U and two O vacancies bound together) trap site [13] and the binding energy and migration barrier in the above equation must be consistent with this characteristic. Similarly, in the $UO_{2+x}$ range we assume that oxidation occurs via $\frac{1}{2}O_2(g) + 2U_U^X + V_I^X \Leftrightarrow O_I'' + 2h^{\bullet}$ ($E_2$) and the corresponding activation energy for Xe diffusion can be written as:

$$E_a^{Xe} = E_S - 2E_{FP_O} - 2\left(\frac{E_{p_{O2}}}{6} - \frac{E_2}{3}\right) + E_m^{V_U,C} - E_B \quad \textbf{(Equation 6)}$$

In this regime Xe occupies the $V_U$ trap site [12] and the migration barrier and binding energy should be defined accordingly.

The parameters entering the above equations are summarized in Table 1. They were all obtained from density functional theory (DFT) calculations according to the methodology outlined in [13,14,16]. Most of these parameters were already published [13], however the $E_m^{V_U,C}$ barriers for the $V_{UO}$ and $V_{UO2}$ traps sites are new. In previous work we assumed that all three $E_m^{V_U,C}$ barriers were identical to the $V_U$ case, which, according to the results in Table 1, does not seem to be an accurate assumption. It is interesting to note that the lowest intra-cluster barrier refers to the case without any oxygen vacancies associated with mobile Xe cluster, which may appear slightly counterintuitive. The Xe activation energies obtained from the $UO_{2-x}$, $UO_2$ and $UO_{2+x}$ models above are listed in Table 2 together with available experimental data from Miekley and Felix [15]. The agreement between the

calculations and experiments is rather good and overall it is improved compared to the prediction in [13], which applied the old chemistry model for the oxygen non-stoichiometry.

Using the same models as for Xe above we have also calculated the activation energies for Kr diffusion. The Kr trap site preference is assumed to be identical to Xe, which implies that the active diffusion mechanisms for Kr should be similar to Xe. The corresponding binding energies and migration barriers are listed in Table 1. The activation energies for Kr diffusion are summarized in Table 2. The Kr activation energy is slightly higher than for Xe, though the difference is rather small. The migration barrier for intra-cluster diffusion of the second U vacancy ( $E_m^{V_U,C}$ ) is smaller for Kr than for Xe. The difference is the largest for Xe/Kr occupying the $V_U$ trap site. This can be explained by the smaller size of the Kr atom compared to Xe. Interestingly, the decrease of the migration barrier is offset by decreasing binding energy of the second U vacancy to the fission gas atom trap site ($E_B$). The net effect is higher Kr activation energy. Experimental measurements on stoichiometric $UO_2$ samples confirm that Kr has a slightly higher diffusivity [8-10].

The high-temperature range (T > 1650 K) in Turnbull's model refers to intrinsic diffusion dominated by thermal vacancies, which thus corresponds to the activation energies summarized in Table 2. We note that for Xe the calculated data agree better with Matzke's (3.9 eV) than with Turnbull's model (3.0 eV). Turnbull relied on experiments due to Davies and Long [11]. The activation energy for Kr in this stoichiometry range is even higher. Nevertheless, the agreement is quite good and allows for a more detailed interpretation of the experimental data than was possible in the absence of these DFT results.

**Table 1: Parameters entering the Xe and Kr activation energy models for fission gas diffusion in $UO_{2-x}$, $UO_2$ and $UO_{2+x}$ (see above). The second value for $E_m^{V_U,C}(V_{UO_2})$ represents binding of a $V_{UO2}$ cluster as mobile defect rather than $V_U$ as assumed for all other cases. This is meant to correspond to irradiation conditions, see text for details. All units are in eV.**

| | $E_{O_I}$ | $E_S$ | $E_{eh}$ | $E_{FP_O}$ | $E_{p_{O2}}$ | $E_1$ | $E_2$ |
|---|---|---|---|---|---|---|---|
| Xe | -0.60 | 7.65 | 1.91 | 4.13 | 5.10 | 8.125 | -1.60 |
| Kr | -0.60 | 7.65 | 1.91 | 4.13 | 5.10 | 8.125 | -1.60 |
| | $E_m^{V_U,C}(V_U)$ | $E_m^{V_U,C}(V_{UO})$ | $E_m^{V_U,C}(V_{UO_2})$ | $E_B(V_U)$ | $E_B(V_{UO})$ | $E_B(V_{UO_2})$ | |
| Xe | 3.40 | 5.20 | 5.48/3.72 | -0.64 | -0.81 | -3.71/-2.31 | |
| Kr | 2.84 | 4.90 | 5.14 | 0.01 | -0.33 | -2.88 | |

**Table 2: Calculated and measured [15] Xe and Kr activation energies. All units are in eV.**

| | $E_a(UO_{2-x})$ | $E_a(UO_2)$ | $E_a(UO_{2+x})$ |
|---|---|---|---|
| Xe Calculated | 5.70 | 3.86 | 1.52 |
| Xe Experimental [15] | 6.0 | 3.9 | 1.7 |
| Kr Calculated | 6.37 | 4.04 | 1.61 |

## Analysis of vacancy enhanced diffusion mechanism

The intermediate temperature range between 1381 and 1650 K was rationalized by irradiation-enhanced diffusion and from experiments the activation energy was determined to be approximately 1.2 eV [8-10]. Fission gas diffusion was assumed to be controlled by uranium vacancies and, using the experimentally determined migration barrier of 2.4 eV, the irradiation enhanced activation energy for fission gas transport was derived as:

$$D_2 = s^2 J_V V$$
$$J_V \propto \exp\left(-\frac{2.4}{k_B T}\right) \quad \text{(Equation 7)}$$
$$V \approx V_{irr} = \sqrt{K'/J_V Z}$$

Here $s$ is the atomic jump distance, $K'$ is the fission rate, $J_V$ is the vacancy flux (under irradiation), $V$ is the vacancy concentration and $V_{irr}$ is the irradiation-induced vacancy concentration and $Z$ is the number of sites around a point defect from which recombination is inevitable. This yields an activation of 1.2 eV, which seemingly agrees well with the value obtained from in-pile experiments.

This derivation deviates slightly from that used above for thermal diffusion. If we assume that the same diffusion mechanism is active for vacancies produced by irradiation as for thermal vacancies the activation energy should be expressed as:

$$D_2 = s^2 J_{Xe} V$$
$$J_{Xe} \propto \exp\left(-\frac{E_m^{Xe_{U_2O}} - E_B^{Xe_{U_2O}}}{k_B T}\right) \quad \text{(Equation 8)}$$
$$V \approx V_{irr} = \sqrt{K'/J_V Z}$$
$$J_V \propto \exp\left(-\frac{E_m^{V_{U_2}}}{k_B T}\right)$$

Here $E_m^{Xe_{U_2O}}$ is the intra-cluster U vacancy migration barrier, $E_B^{Xe_{U_2O}}$ is the binding energy of a U vacancy to the $V_{UO}$ Xe trap site and $E_m^{V_{U_2}}$ is the migration barrier for U U divacancy clusters, which dominate diffusion in irradiated materials [13]. Using the DFT data in Table 1 we obtained activation energy of 3.17 eV, which is significantly larger than the experimental value in the intermediate temperature regime (1.19 eV, blue line in Fig. 1). This poor agreement strongly suggests that there is another diffusion mechanism responsible for the measured activation energy in the intermediate temperature regime. The first option that we investigated was formation of mobile clusters consisting of Xe occupying the $V_{UO2}$ site and an additional $V_{UO2}$ defect acting as the mobile defect. The existence of such defects under irradiation is motivated by the high concentration of oxygen defects

and the strong binding between oxygen vacancies and U vacancies as well as between oxygen vacancies and Xe trap sites. The oxygen vacancies would eventually annihilate since they are not thermodynamically stable (except for $UO_{2-x}$), but it is not unreasonable that they exist bound to other defects long enough to enable the larger clusters to diffuse. For this cluster we calculated a barrier of 3.72 eV and a binding energy of 2.30 eV. Applying these numbers we obtain activation energy of -0.03 eV, which is much lower than experiments. However, if the concentration of irradiation-induced vacancies is assumed to be a constant rather than having the $1/J_V$ dependence postulated above, we obtain 1.27 eV in rather good agreement with the experimental data. Additional work is needed to motivate using a constant value for the irradiation induced vacancy concentration. The $1/J_V$ dependence originates from the time-dependence of the vacancy annealing process; however since Xe atoms would effectively act as sinks it is not immediately obvious why this term should be included in the calculation of vacancies available for clustering. A related mechanism would be for Xe to occupy the $V_{UO2}$ trap site, while binding a single U vacancy. This yields activation energy of 0.38 eV.

Another possibility is that, due to the strong interaction between fission gas atoms and vacancies produced by irradiation they will form extended clusters filled by Xe atoms. These clusters may diffuse via random walk or along a gradient such as concentration or temperature. The rate-limiting step for this process will depend on the size of the cluster. First we tried to calculate the internal vacancy migration barrier for clusters containing one Xe atom and at least three U vacancies. However, this approach was not very successful due to the complexity and limitations of DFT for large supercells. The results that we obtained suggested that the barrier was strongly dependent on the cluster configuration and there were no indications of barriers lower than that for Xe in a single U vacancy ($V_U$). However, these conclusions should be treated with some care since the simulation setup was reaching the limit of what is possible with DFT.

Below we investigate surface diffusion of U atoms, which could be the rate-limiting step for bubbles that has reached a certain size. Additional work is required to establish the limits for this mechanism.

### Surface controlled motion of fission gas bubbles

The most stable $UO_2$ surface is the (111) surface. It is consequently reasonable to assume that voids and fission gas bubbles formed due to irradiation would be terminated by (111) $UO_2$ surfaces. Both voids and fission gas bubbles could move their centre of mass (diffuse) by moving U atoms from one side to another. This process may take place either by subsurface diffusion of U vacancies or surface diffusion of U ad-atoms, possibly coordinated with oxygen vacancies (for sub-surface vacancies) or ad-atoms (for U ad-atoms). We simulated both of these possibilities by using a using a periodic slab of $UO_2$ ($[0.5\ 0.0\ -0.5]_{Fluorite}$, $[-0.75\ 0.75\ 0.0]_{Fluorite}$, $[1.0\ 1.0\ 1.0]_{Fluorite}$) separated by vacuum along the third dimension. This setup is illustrated in Fig. 2. The barriers for subsurface diffusion of U vacancies or

clusters of U and O vacancies are about 1 eV lower than the corresponding bulk barriers (3.4 eV compared to 4.8 eV for bulk vacancies). The migration of U ad-atoms or a neutral cluster of one uranium and two oxygen atoms was calculated to have a barrier of 1.01 and 1.25 eV, respectively. The corresponding migration pathways are shown in Fig. 2. Both of these numbers are very close to the measured activation energy in the intermediate temperature regime of Turnbull's model [8-10]. If this agreement is accurate, it indicates that Xe transport may be controlled by small fission gas bubbles or extended clusters rather than by bulk diffusion via vacancies produced by irradiation. For this to be possible enough defects must be generated to create fission gas bubbles and the ad-atoms or ledges responsible for surface diffusion. Fission gas bubbles are formed during in-pile conditions and then destroyed by resolution via collision with fission fragments. This means that the conditions for surface controlled bubble diffusion may exist. Additional work is required to determine whether $V_{UO2}$ cluster diffusion or bubble diffusion mechanism is responsible for the in-pile activation energies for fission gas diffusion in the intermediate temperature range.

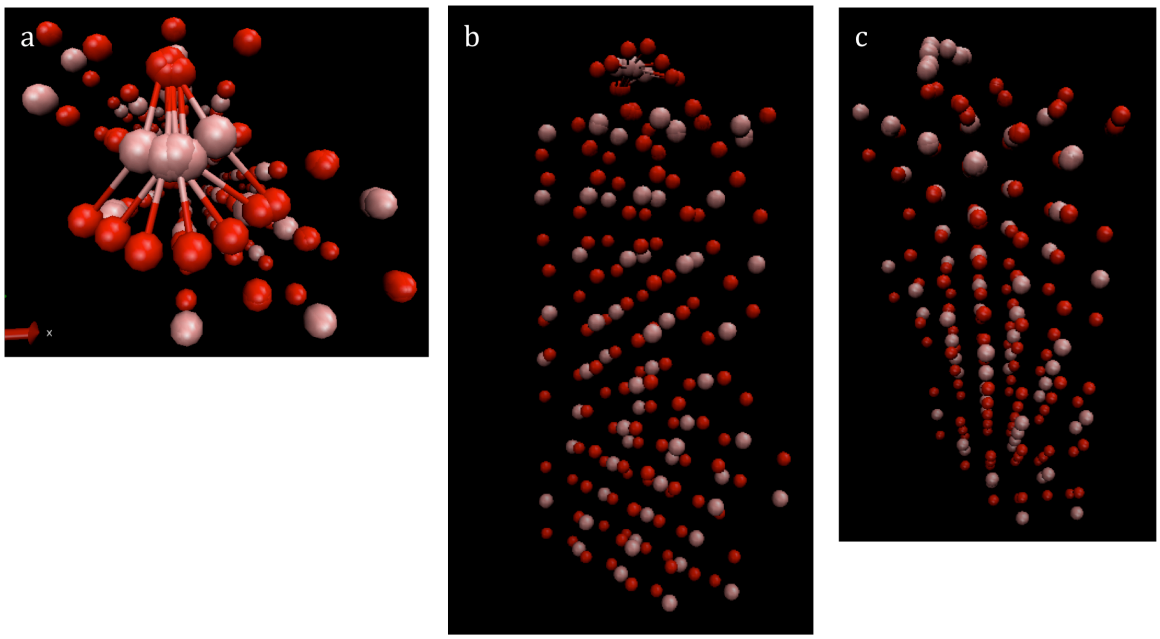


**Figure 2: Surface diffusion mechanisms simulated using (111) $UO_2$ slabs separate by vacuum. a) Top view of the migration path of a O-U-O ad-atom cluster. b) The same mechanism viewed from the side. C) The migration mechanism of a U ad-atom.**

## Conclusions

We have reported density functional theory (DFT) calculations of the activation energy for Xe diffusion in bulk $UO_{2\pm x}$, which included an improved model for the impact of chemistry on the $UO_{2\pm x}$ non-stoichiometry and new data for intra-cluster diffusion of U vacancies. Good agreement was found with available experimental data. A similar analysis was performed for diffusion of Kr, which was predicted to behave very similar to Xe but generally with slightly higher activation energy. Based on the DFT data for Xe and U vacancy diffusion we have analyzed the existing fission gas release models due to Massih-Forsberg and Turnbull. Since the DFT data hinted

at some inconsistencies with available experiments, we investigated alternative mechanisms for irradiation enhanced fission gas transport. In particular we calculated the rate limiting steps for U surface diffusion and for diffusion mediated by bound Schottky defects. In the first case we obtained a migration barrier in good agreement with the experimental activation energy and in the second case we also obtained activation energy in good agreement with experiments if the irradiation induced vacancy concentration is approximately independent of temperature. Future work will elucidate these mechanisms in more detail and try to determine their validity.

## References


1. A. H. Booth, A method of calculating gas diffusion from $UO_2$ fuel and its application to the X-2-f test, Technical Report AECL 496 CRDC-721, Atomic Energy of Canada Limited (1957).
2. M. V. Speight, Nucl. Sci. Eng. **37**, 180 (1969).
3. K. Forsberg and A. R. Massih, J. Nucl. Mater. **135**, 140 (1985).
4. K. Forsberg and A. R. Massih, J. Nucl. Mater. **127**, 141 (1985).
5. K. Forsberg and A. R. Massih, Modelling Simul. Mater. Sci. Eng. **15**, 335 (2007).
6. D. D. Lanning, C. E. Beyer and C. L. Painter, "FRAPCON-3: Modifications to Fuel Rod Material Properties and Performance Models for High-Burnup Application" (1997).
7. R. J. White and M. O. Tucker, J. Nucl. Mater. **118**, 1 (1983).
8. J. A. Turnbull, J. Nucl. Mater. **50**, 63 (1974).
9. J. A. Tumbull and C.A. Friskney, J. Nucl. Mater. **71**, 238 (1978).
10. J. A. Turnbull, C. A. Friskney, J. R. Findlay, F. A. Johnson and A. J. Walter, J. Nucl. Mater. **107**, 168 (1982).
11. D. Davies and G. Long, AERE Rep. No. 4347 (1963).
12. H. J. Matzke, Radiat. Eff. Defect S. **53**, 219 (1980).
13. D. A. Andersson, B. P. Uberuaga, P. V. Nerikar, C. Unal and C. R. Stanek, Phys. Rev. B **84**, 054105 (2011).
14. B. Dorado, D. A. Andersson, C. R. Stanek, M. Bertolus, B. P. Uberuaga, G. Martin, M. Freyss and P. Garcia, Phys. Rev. B **86**, 035110 (2012).
15. W. Miekeley and F. W. Felix, J. Nucl. Mater. **42,** 297 (1972).
16. D. A. Andersson, F. J. Espinosa-Faller, B. P. Uberuaga and S. D. Conradson, J. Chem. Phys. **136**, 234702 (2012).